Applied Physics Letters ARTICLE scitation.org/journal/apl

Enhancement of 2DEG effective mass in AlN/$Al_{0.78}Ga_{0.22}N$ high electron mobility transistor structure determined by THz optical Hall effect

Cite as: Appl. Phys. Lett. **120**, 253102 (2022); doi: 10.1063/5.0087033
Submitted: 31 January 2022 · Accepted: 25 May 2022 ·
Published Online: 24 June 2022

View Online Export Citation CrossMark

Philipp Kühne,[1,2,3,a] Nerijus Armakavicius,[1,2,3] Alexis Papamichail,[1,2,3] Dat Q. Tran,[2,3] Vallery Stanishev,[1,2,3] Mathias Schubert,[1,2,3,4] Plamen P. Paskov,[2,3] and Vanya Darakchieva[1,2,3,5]

AFFILIATIONS

[1]Terahertz Materials Analysis Center (TheMAC), Linköping University, 581 83 Linköping, Sweden
[2]Center for III-Nitride Technology, C3NiT—Janzén, Linköping University, 581 83 Linköping, Sweden
[3]Department of Physics, Chemistry and Biology (IFM), Linköping University, 581 83 Linköping, Sweden
[4]Department of Electrical and Computer Engineering, University of Nebraska-Lincoln, Lincoln, Nebraska 68588, USA
[5]NanoLund and Solid State Physics, Lund University, 22100 Lund, Sweden

Note: This paper is part of the APL Special Collection on Wide- and Ultrawide-Bandgap Electronic Semiconductor Devices.
[a]**Author to whom correspondence should be addressed:** philipp.kuhne@liu.se

ABSTRACT

We report on the free charge carrier properties of a two-dimensional electron gas (2DEG) in an AlN/$Al_xGa_{1-x}N$ high electron mobility transistor structure with a high aluminum content ($x = 0.78$). The 2DEG sheet density $N_s = (7.3 \pm 0.7) \times 10^{12}$ cm^{-2}, sheet mobility $\mu_s = (270 \pm 40)$ cm^2/(Vs), sheet resistance $R_s = (3200 \pm 500)$ Ω/□, and effective mass $m_{\text{eff}} = (0.63 \pm 0.04)m_0$ at low temperatures ($T = 5$ K) are determined by terahertz (THz) optical Hall effect measurements. The experimental 2DEG mobility in the channel is found within the expected range, and the sheet carrier density is in good agreement with self-consistent Poisson–Schrödinger calculations. However, a significant increase in the effective mass of 2DEG electrons at low temperatures is found in comparison with the respective value in bulk $Al_{0.78}Ga_{22}N$ ($m_{\text{eff}} = 0.334\, m_0$). Possible mechanisms for the enhanced 2DEG effective mass parameter are discussed and quantified using self-consistent Poisson–Schrödinger calculations.

Ultra-wide-bandgap semiconductors, such as $Al_xGa_{1-x}N$ with high Al-content, are very promising materials for next generation high-power electronic devices. A common way to compare the potential material performance are figures of merit, such as the unipolar and lateral figures of merit (UFOM and LFOM), indicating that materials minimize conduction losses in low-frequency unipolar and lateral device structures, respectively.[1,2] The Johnson figure of merit (JFOM) indicates a material's suitability for high frequency power transistor applications. While the JFOM of AlGaN outperforms GaN for any Al-content,[3] simulations of the UFOM and LOFM at room temperature for AlGaN show that this is only the case for an Al-composition of $x > 0.7$ and $x > 0.9$, respectively.[4,5] However, the typical temperatures at which devices operate are much higher. For example, at 500 K, the UFOM and LFOM of AlGaN exceed the FOMs of GaN at $x > 0.3$ and $x > 0.65$, respectively.[4,6,7] Furthermore, it is reasonable to assume that for very high Al-compositions ($x > 0.9$), the conduction band offset at the AlN/AlGaN interface is not large enough anymore to provide sufficient confinement for the two-dimensional electron gas (2DEG) that can form at the interface in high electron mobility transistors (HEMTs).[8] However, HEMTs with $Al_xGa_{1-x}N$ channels with slightly lower Al-content of $0.7 < x < 0.9$ are of interest for future high-power and high-frequency devices. Though there are numerous publications reporting device structures with AlGaN 2DEG channels,[9–19] only few demonstrate structures with high Al-content $x \geq 0.7$.[8,20–22]

Despite progress in the growth of such devices, achievement of low Ohmic contact resistances, while maintaining the 2DEG in the channel, is still challenging.[23] High Al-content AlGaN has a low electron affinity (in AlN the electron affinity is 0.6 eV) that naturally leads

to large Schottky barriers.[24] Methods to achieve Ohmic contacts include, among others, adding a heavily doped GaN cap layer, adding composition graded contact layers,[25] or using regrown Ohmic contacts.[26] However, high Ohmic contact resistance often remains the main factor that degrades device performance.[10–12,17] The optical Hall effect (OHE) is a contactless method for accurate determination of bulk free charge carrier and 2DEG properties and can be employed to study high Al-content AlGaN structures avoiding the issues with contacts.[27] The OHE essentially combines generalized ellipsometry at long wavelengths with high static magnetic fields, allowing to characterize free charge carrier properties at frequencies relevant for device applications. Previously, the OHE was successfully employed for the determination of 2DEG properties in $Al_{0.26}Ga_{0.74}N$/GaN structures by Schöche *et al.*[28] and for their temperature dependence in $Al_{0.25}Ga_{0.75}N$/GaN structures by Hofmann *et al.*[29] A cavity enhanced OHE was demonstrated on $Al_{0.82}In_{0.18}N$/AlN/GaN[30,31] and on $Al_xGa_{1-x}N$/AlN/GaN ($x = 0.19$ and $x = 0.25$) HEMT structures.[32,33] OHE data analysis was discussed by Schubert *et al.*[27]

In this work, we present contactless characterization of 2DEG properties in an AlN/$Al_xGa_{1-x}N$ HEMT with a high Al-content ($x = 0.78$) channel. The free charge carrier parameters of the 2DEG are extracted from THz OHE measurements and discussed using results obtained in this Letter from self-consistent Poisson–Schrödinger calculations.

The HEMT structure was grown in a hot-wall metal-organic chemical vapor deposition (MOCVD) reactor on a semi-insulating 4H-SiC (0001) substrate with a nominal thickness of 500 μm. First, a 250 nm-thick AlN nucleation layer was grown at 1200 °C, followed by a 100 nm-thick $Al_xGa_{1-x}N$ graded layer grown as the temperature was reduced from 1200 to 1040 °C.[34] Then, a 400-nm-thick $Al_xGa_{1-x}N$ layer with $x = 0.78$ was grown at 1040 °C. Finally, an AlN barrier with the thickness of 10 nm was grown at 1040 °C. A 2DEG forms at the AlN/$Al_xGa_{1-x}N$ interface for which the roughness is expected to be comparable to the surface roughness of an identical sample structure without the AlN barrier with the root mean square (RMS) of 0.67 nm determined over a 3×3 μm^2 area.

The THz OHE measurements were employed to determine the free charge carrier properties of the 2DEG channel, using an in-house built THz ellipsometer.[33] The sample was mounted in a cavity enhanced (CE) configuration[30] on an aluminum plate, using adhesive tape spacers providing a nominal cavity thickness of 100 μm. The sample was loaded into a superconducting 8 T magnet with optical ports and cooled to a temperature of $T = 5$ K. Mueller matrix spectra[35] M^0 and M^+ at magnetic fields of $B = 0$ T and $B = 8$ T, respectively, were recorded in the reflection configuration at an angle of incidence of $\Phi = 45°$, with the magnetic field parallel to the incoming THz beam. For data analysis, OHE difference spectra $\delta M^+ = M^+ - M^0$ were calculated.

Figure 1 shows a high-resolution x-ray diffraction (HRXRD) reciprocal space map (RSM) around the $10\bar{1}5$ reciprocal lattice point. Analysis confirms the Al-content of $x = 0.78$ in the channel layer. Also, in- and out-of-plain strain of $\varepsilon_c = 0.0003$ and $\varepsilon_a = 0.0004$, respectively, are determined, indicating that the $Al_xGa_{1-x}N$ layer is highly relaxed. The sample is crack-free thanks to the strain management via the graded AlGaN buffer layer.

OHE data analysis in the THz spectral range was performed employing stratified layer model calculations, using the 4×4 matrix

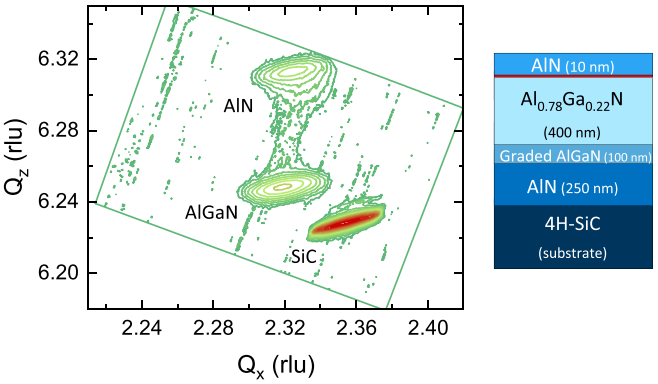

FIG. 1. HRXRD reciprocal space map around the asymmetric $10\bar{1}5$ reciprocal lattice point for the AlN/$Al_{0.78}Ga_{0.22}N$/SiC HEMT structure. The lateral (perpendicular to the *c*-axis) and vertical (along the *c*-axis) scattering vectors Q_x and Q_z are given in reciprocal lattice units (rlu) with dimension of $2\pi/\lambda$, where $\lambda = 1.540\,597\,4$ Å. The sample structure is indicated on the right.

formalism,[35] in combination with the Levenberg–Marquardt algorithm and parametrized model dielectric functions.[27] The model consists of a semi-infinite layer for the metal backside, a void gap with variable thickness for the backside cavity, a uniaxial layer with variable thickness for the 4H-SiC substrate, and a layer with a fixed thickness of $d = 1$ nm for the 2DEG channel. Due to the large ratio of the wavelength to the product of index of refraction and layer thickness ($\lambda \gg nd$), all other layers present in the sample structure only add minor contributions to the ellipsometry spectrum and can, therefore, be neglected. The optical properties of the metal backside are modeled with a classic Drude dielectric function with free charge carrier density $N = 10^{23}$ cm^{-3}, mobility $\mu = 5\,cm^2/(V\,s)$, and effective mass $m_{eff} = m_0$, where m_0 is the free electron mass. The index of refraction of the backside cavity is set to $n = 1$. The 4H-SiC substrate has a hexagonal crystal structure and is, therefore, optically anisotropic (uniaxial). Its THz optical properties are determined by measuring a bare substrate to be $n_\perp = 3.13$ and $n_\parallel = 3.20$, for the in- and out-of-plane indices of refraction, respectively. The optical response of the 2DEG channel is modeled by a dielectric tensor based on the Drude model augmented by a term accounting for the influence of the Lorentz force. Instead of the volume carrier density, we determine the sheet carrier density $N_s = dN$, where d is a virtual optical thickness of the 2DEG and N is a virtual three dimensional charge carrier density. In our OHE experiment, we only detect information related to N_s. This can be best understood when inspecting the mathematical formalism, which is used to analyze our OHE data. A partial 4×4 transfer matrix is composed representing every physical layer in the layer stack,[35] $T_p = \exp\left(i\frac{\omega}{c}\Delta d\right)$. For ultra thin layers, $\lambda \gg d$, e.g., for a 2DEG at THz frequencies. It can be shown that all resulting OHE spectra regardless of whether measured in reflection or transmission, for ultra thin layers, are only proportional to and dependent on the product dN, hence, N_s, while no sensitivity is contained in the optical data to differentiate d and N. Further model parameters include a small offset parameter for the angle of incidence and a calibration offset for the polarizer. Best-model calculations are performed by varying the parameters named above together with the sheet carrier density N_s, mobility μ, and electron effective mass m_{eff} of the 2DEG channel.

More details on the principles of OHE data analysis together with relevant optical models are given in Ref. 27.

Experimental data together with best-model calculations are presented in Fig. 2. We find a good agreement between experimental (blue squares) and best-model calculated (red lines) data. The pronounced feature at $\nu \approx 0.8$ THz is induced by a Fabry–Pérot interference in the 4H-SiC substrate and backside cavity. The spectral location of the feature is determined by the substrate and backside cavity thicknesses, while the line shape and amplitude are strongly influenced by the 2DEG free charge carrier properties. The block-off diagonal elements $\delta M^{+}_{13,31}$ and $\delta M^{+}_{23,32}$ deviation from zero are indicative of cross-polarization emerging from the sample under linear polarized light illumination at the given frequency. Furthermore, these matrix elements vanish for $B = 0$ T. Therefore, the appearance of cross polarization for $B \neq 0$, in a stack of optically isotropic layers, is caused by the magnetic field (Lorentz force). This confirms the existence of a channel with free charge carriers. Additionally, the sign of the features in the OHE data (e.g., the maximum in δM^{+}_{32}) indicates that electrons are present in the sample.

The best-model parameters for the angle of incident offset and the calibration offset for the polarizer are $\delta\Phi = (1.8 \pm 0.1)^\circ$ and $\Theta_p = (-0.09 \pm 0.01)^\circ$, respectively. The thicknesses of the backside cavity and the 4H-SiC substrate are $d_{\mathrm{cavity}} = (114.3 \pm 0.4)$ μm and $d_{\mathrm{SiC}} = (494.0 \pm 0.1)$ μm, respectively, which is in good agreement with the nominal values. The best model has a mean squared error (MSE) of MSE = 1.44, it yields a sheet carrier density of the 2DEG of $N_s = (7.3 \pm 0.7) \times 10^{12}$ cm^{-2}, a sheet mobility of $\mu_s = (270 \pm 40)$ cm^2/(V · s), a sheet resistance of $R_s = (3200 \pm 500)$ $\Omega/\square$, and an effective mass of $m_{\mathrm{eff}} = (0.63 \pm 0.04) m_0$.

We conducted simulations of the HEMT structure under investigation employing self-consistent Poisson–Schrödinger calculations.[36,37] The conduction band offset is assumed to be 65% of the difference between AlN and $Al_{0.78}Ga_{0.22}N$ bandgaps.[38] For $Al_{0.78}Ga_{0.22}N$, the bandgap energy is obtained by interpolation between values of the binary compounds at T = 5 K with a bowing parameter of 0.8 eV. The bandgap of AlN and $Al_{0.78}Ga_{0.22}N$ is corrected for the strain measured in the layers. Figure 3(a) displays the charge carrier distribution in the vicinity of the AlN/$Al_{0.78}Ga_{0.22}N$ interface and (b) the conduction band profile together with the quantized energy levels in the triangular quantum well. In the case of a fully relaxed $Al_{0.78}Ga_{0.22}N$ layer, the sheet carrier density is calculated as $N_s = 2 \times 10^{13}$ cm^{-1}, which is about twice as high as the value extracted from our OHE data. Furthermore, capacitance–voltage (C–V) measurements were performed using a Hg-probe setup with a 4284A LCR meter from Agilent. A sheet carrier density of $N_s = 5.2 \times 10^{12}$ cm^{-2} was determined at room temperature. This value is very similar to the low-temperature N_s obtained from the OHE, and it further validates our results, since for polarization doping, only a small temperature dependency of 2DEG density is expected.

Comparing with the conventional $Al_{0.19}Ga_{0.81}N$/GaN HEMT structures,[32] the sheet mobility measured in AlN/$Al_{0.78}Ga_{0.22}N$ HEMT is significantly lower. Note that here the 2DEG is located in the $Al_{0.78}Ga_{0.22}N$, where the mobility is mainly limited by alloy scattering.[4,23,39] The mobility value that we measure is at $T = 5$ K, while literature data for similar device structures are typically determined at or above room temperature. The alloy scattering is the limiting scattering mechanism up to room temperature.[4,5] Its contribution to the total mobility has been predicted to follow a $T^{-1/2}$ dependence.[40] Using

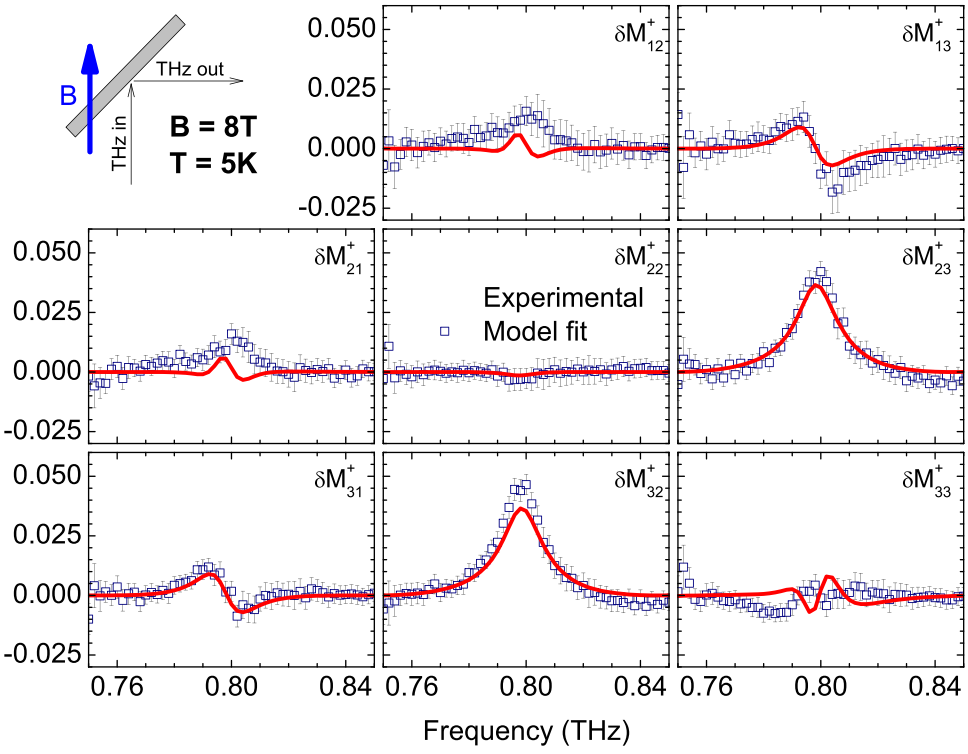

FIG. 2. Best-model (red lines) and experimental (blue squares) cavity enhanced OHE difference spectra $\delta M^{+} = M^{+} - M^{0}$ (M^{+}: Mueller matrix data at positive field; M^{0}: Mueller matrix data at zero field) for AlN/$Al_{0.78}Ga_{0.22}N$ HEMT structure at $\Phi = 45^\circ$, $T = 5$ K and $B = 8$ T, with the magnetic field parallel to the incident THz beam. The inset on top indicates the sample configuration during OHE measurements.

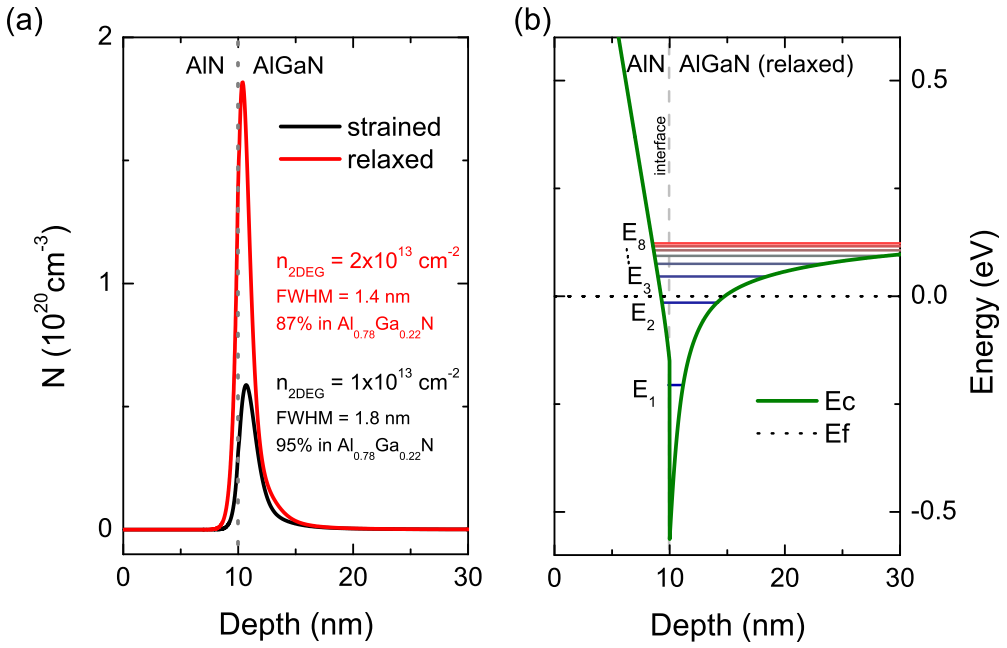

FIG. 3. (a) Charge carrier distribution in the vicinity of the AlN/AlGaN interface, obtained by the self-consistent solution of the one-dimensional Poisson–Schrödinger equation. Calculations for the charge carrier distribution are shown for strained and fully relaxed $Al_{0.78}Ga_{0.22}N$. (b) Conduction band profile and quantized energy levels for the same structure, where the $Al_{0.78}Ga_{0.22}N$ layer is assumed to be relaxed.

this relation, we extrapolate a room temperature mobility of $\mu_{s,300\,K} = 35\,cm^2/(V \cdot s)$, which is in good agreement with calculations for $Al_{0.78}Ga_{0.22}N$ from Coltrin *et al.*,[5] but lower than the value obtained by Bajaj *et al.*[4] In our case, the room temperature free charge carrier properties could not be determined due to the lower mobility value resulting in OHE signatures in Mueller matrix spectra below the signal-to-noise ratio of our system.

The effective mass determined here is significantly higher than the value measured recently by Schöche *et al.* using mid-infrared OHE for epitaxial Si-doped $Al_{0.79}Ga_{0.21}N$ layers ($m_{eff} = 0.334\,m_0$).[41] The discrepancy may be due to (i) the enhancement of the effective mass due to hybridization, conduction band non-parabolicity, the electron–phonon coupling (polaronic effect) in the case of two-dimensional (2D) structures,[42,43] and/or (ii) the possible existence of physical mechanisms at THz frequencies in 2DEG channels, which are not accounted for by the Drude model for quasi-free electrons involved here in our analysis.

In order to quantify possible mass enhancement phenomena, self-consistent Poisson–Schrödinger calculations are performed. Our calculations provide the space distribution of the 2DEG at AlN/$Al_{0.78}Ga_{0.22}N$ interface as well as the probability p_{AlN} for the electron wave function to penetrate into the AlN barrier. For a relaxed $Al_{0.78}Ga_{0.22}N$ layer, we found that $p_{AlN} = 13\%$. The hybridized effective mass can be calculated using $1/m = p_{AlN}/m_{AlN} + p_{AlGaN}/m_{AlGaN}$,[44] which leads to an increase by 2%. The effect of the conduction band non-parabolicity can be roughly estimated by $m^*_{eff} = m_{eff}(1 + \frac{2E_0}{3E_g})$,[44–46] where E_0 is the sum of the kinetic energy of the electrons in the triangular well and the Fermi energy and E_g is the bandgap energy. The non-parabolicity is found to increase the effective mass by 7%. The polaronic contribution to the electron effective mass is estimated in the case of 2D electrons with a weak phonon coupling[44,47,48] $m^*_{eff} = m_{eff}\left(1 + \frac{\pi}{8}\alpha + 0.127\alpha^2\right)$, where α is the Fröhlich polaron coupling parameter. To evaluate the magnitude of the polaronic effect, we use the Fröhlich coupling parameter for AlN, $\alpha = 0.75$,[49] and obtain 36% increase in the effective mass. Combining all effects, the electron effective mass of $m^*_{eff} = 0.50$ is estimated. However, this value serves as an upper limit, since the polaronic effect should be reduced due to screening at the carrier concentration determined.[44,50] Hence, our OHE result of $m_{eff} = (0.63 \pm 0.04)m_0$ is still substantially larger than the possible effective mass enhanced by polaronic, non-parabolicity, and hybridization effects. At this point, we have no explanation for this observation, and we believe that potentially, physical processes not presently included into our OHE model analysis may be responsible for the observed mass enhancement at THz frequencies at very large Al-content AlGaN/GaN HEMT 2DEG structures. Future work is proposed to study the temperature dependence of charge carrier properties and high frequency electrical properties.

We studied the free charge carrier properties of 2DEG in an AlN/$Al_{0.78}Ga_{0.22}N$ HEMT structure at low temperature ($T = 5\,K$) employing the THz optical Hall effect and compared the results with self-consistent Poisson–Schrödinger calculations. While the measured 2DEG sheet density of $N_s = (7.3 \pm 0.7) \times 10^{12}\ cm^{-2}$ is in good agreement with our self-consistent Poisson–Schrödinger calculations, and the low temperature sheet mobility of $\mu_s = (270 \pm 40)\,cm^2/(V \cdot s)$ falls within the expected range, the extracted electron effective mass value of $m_{eff} = (0.63 \pm 0.04)m_0$ is significantly higher than what is reported in the literature for bulk $Al_{0.78}Ga_{0.22}N$ layers.[41] The observed

enhancement of the electron effective mass is attributed to the combined effects of the hybridization, conduction band non-parabolicity, and electron–phonon coupling. However, physical mechanisms not accounted for in our OHE model analysis cannot be ruled out.

This work was performed within the framework of the Center for III-Nitride Technology, C3NiT-Janzén, supported by the Swedish Governmental Agency for Innovation Systems (VINNOVA) under the Competence Center Program Grant No. 2016-05190, Linköping University, Chalmers University of technology, Ericsson, Epiluvac, FMV, Gotmic, Hitachi Energy Research, Hexagem, On Semiconductor, Saab, SweGaN, United Monolithic Semiconductors (UMS), and Volvo Cars. We further acknowledge support from the Swedish Research Council Vetenskapsrådet (VR) under Grant No. 2016-00889, Swedish Foundation for Strategic Research under Grants Nos. RIF14-055 and EM16-0024, and the Swedish Government Strategic Research Area in Materials Science on Functional Materials at Linköping University, Faculty Grant Stark forskningsmiljö (SFO) Mat LiU No. 2009-00971. This work was supported in part by the National Science Foundation under Award Nos. DMR 1808715 and OIA-2044049, and by the Air Force Office of Scientific Research under Award Nos. FA9550-18-1-0360, FA9550-19-S-0003, and FA9550-21-1-0259.

AUTHOR DECLARATIONS

Conflict of Interest

The authors have no conflicts to disclose.

Author Contributions

Philipp Kühne: Data curation (lead); formal analysis (lead); investigation (lead); methodology (lead); project administration (lead); validation (lead); visualization (lead); writing – original draft (lead); writing – review & editing (lead). **Nerijus Armakavicius:** Methodology (equal); writing – review & editing (equal). **Alexis Papamichail:** Methodology (equal); resources (equal); writing – review & editing (equal). **Dat Q. Tran:** Data curation (supporting); formal analysis (supporting); writing – review & editing (supporting). **Vallery Stanishev:** Investigation (equal); methodology (equal); writing – review & editing (equal). **Mathias Schubert:** Funding acquisition (equal); methodology (equal); writing – review & editing (equal). **Plamen P. Paskov:** Formal analysis (equal); investigation (equal); methodology (equal); writing – original draft (equal); writing – review & editing (equal). **Vanya Darakchieva:** Conceptualization (equal); funding acquisition (equal); project administration (equal); supervision (equal); writing – original draft (equal); writing – review & editing (equal).

DATA AVAILABILITY

The data that support the findings of this study are available from the corresponding author upon reasonable request.

REFERENCES

[1]R. J. Kaplar, A. A. Allerman, A. M. Armstrong, M. H. Crawford, J. R. Dickerson, A. J. Fischer, A. G. Baca, and E. A. Douglas, ECS J. Solid State Sci. Technol. **6**, Q3061 (2017).
[2]A. G. Baca, A. M. Armstrong, B. A. Klein, A. A. Allerman, E. A. Douglas, and R. J. Kaplar, J. Vac. Sci. Technol. A **38**, 020803 (2020).
[3]M. E. Coltrin, A. G. Baca, and R. J. Kaplar, ECS J. Solid State Sci. Technol. **6**, S3114 (2017).
[4]S. Bajaj, T.-H. Hung, F. Akyol, D. Nath, and S. Rajan, Appl. Phys. Lett. **105**, 263503 (2014).
[5]M. E. Coltrin and R. J. Kaplar, J. Appl. Phys. **121**, 055706 (2017).
[6]S. Hashimoto, K. Akita, Y. Yamamoto, M. Ueno, T. Nakamura, K. Takeda, M. Iwaya, Y. Honda, and H. Amano, Phys. Status Solidi A **209**, 501 (2012).
[7]P. H. Carey, F. Ren, A. G. Baca, B. A. Klein, A. A. Allerman, A. M. Armstrong, E. A. Douglas, R. J. Kaplar, P. G. Kotula, and S. J. Pearton, IEEE Trans. Semicond. Manuf. **32**, 473 (2019).
[8]A. G. Baca, A. M. Armstrong, A. A. Allerman, E. A. Douglas, C. A. Sanchez, M. P. King, M. E. Coltrin, T. R. Fortune, and R. J. Kaplar, Appl. Phys. Lett. **109**, 033509 (2016).
[9]T. Nanjo, M. Takeuchi, M. Suita, Y. Abe, T. Oishi, Y. Tokuda, and Y. Aoyagi, Appl. Phys. Express **1**, 011101 (2008).
[10]A. Raman, S. Dasgupta, S. Rajan, J. S. Speck, and U. K. Mishra, Jpn. J. Appl. Phys. **47**, 3359 (2008).
[11]T. Nanjo, M. Takeuchi, M. Suita, T. Oishi, Y. Abe, Y. Tokuda, and Y. Aoyagi, Appl. Phys. Lett. **92**, 263502 (2008).
[12]H. Tokuda, M. Hatano, N. Yafune, S. Hashimoto, K. Akita, Y. Yamamoto, and M. Kuzuhara, Appl. Phys. Express **3**, 121003 (2010).
[13]T. Nanjo, M. Takeuchi, A. Imai, M. Suita, T. Oishi, Y. Abe, E. Yagyu, T. Kurata, Y. Tokuda, and Y. Aoyagi, Electron. Lett. **45**, 1346 (2009).
[14]T. Nanjo, A. Imai, Y. Suzuki, Y. Abe, T. Oishi, M. Suita, E. Yagyu, and Y. Tokuda, IEEE Trans. Electron Devices **60**, 1046 (2013).
[15]A. G. Baca, A. M. Armstrong, A. A. Allerman, B. A. Klein, E. A. Douglas, C. A. Sanchez, and T. R. Fortune, ECS J. Solid State Sci. Technol. **6**, S3010 (2017).
[16]E. A. Douglas, B. Klein, A. A. Allerman, A. G. Baca, T. Fortune, and A. M. Armstrong, J. Vac. Sci. Technol. B **37**, 021208 (2019).
[17]N. Yafune, S. Hashimoto, K. Akita, Y. Yamamoto, H. Tokuda, and M. Kuzuhara, Electron. Lett. **50**, 211 (2014).
[18]H. Xue, C. H. Lee, K. Hussian, T. Razzak, M. Abdullah, Z. Xia, S. H. Sohel, A. Khan, S. Rajan, and W. Lu, Appl. Phys. Express **12**, 066502 (2019).
[19]S. Muhtadi, S. M. Hwang, A. Coleman, F. Asif, G. Simin, M. Chandrashekhar, and A. Khan, IEEE Electron Device Lett. **38**, 914 (2017).
[20]A. G. Baca, B. A. Klein, A. A. Allerman, A. M. Armstrong, E. A. Douglas, C. A. Stephenson, T. R. Fortune, and R. J. Kaplar, ECS J. Solid State Sci. Technol. **6**, Q161 (2017).
[21]B. A. Klein, E. A. Douglas, A. M. Armstrong, A. A. Allerman, V. M. Abate, T. R. Fortune, and A. G. Baca, Appl. Phys. Lett. **114**, 112104 (2019).
[22]A. G. Baca, B. A. Klein, J. R. Wendt, S. M. Lepkowski, C. D. Nordquist, A. M. Armstrong, A. A. Allerman, E. A. Douglas, and R. J. Kaplar, IEEE Electron Device Lett. **40**(1), 17–20 (2019).
[23]A. M. Armstrong, B. A. Klein, A. Colon, A. A. Allerman, E. A. Douglas, A. G. Baca, T. R. Fortune, V. M. Abate, S. Bajaj, and S. Rajan, Jpn. J. Appl. Phys. **57**, 074103 (2018).
[24]H. Xue, S. Hwang, T. Razzak, C. Lee, G. Calderon Ortiz, Z. Xia, S. Hasan Sohel, J. Hwang, S. Rajan, A. Khan, and W. Lu, Solid State Electron. **164**, 107696 (2020).
[25]S. Bajaj, F. Akyol, S. Krishnamoorthy, Y. Zhang, and S. Rajan, Appl. Phys. Lett. **109**, 133508 (2016).
[26]I. Abid, J. Mehta, Y. Cordier, J. Derluyn, S. Degroote, H. Miyake, and F. Medjdoub, Electronics **10**, 635 (2021).
[27]M. Schubert, P. Kühne, V. Darakchieva, and T. Hofmann, J. Opt. Soc. Am. A **33**, 1553 (2016).
[28]S. Schöche, J. Shi, A. Boosalis, P. Kühne, C. M. Herzinger, J. A. Woollam, W. J. Schaff, L. F. Eastman, M. Schubert, and T. Hofmann, Appl. Phys. Lett. **98**, 092103 (2011).
[29]T. Hofmann, P. Kühne, S. Schöche, J.-T. Chen, U. Forsberg, E. Janzén, N. Ben Sedrine, C. M. Herzinger, J. A. Woollam, M. Schubert, and V. Darakchieva, Appl. Phys. Lett. **101**, 192102 (2012).
[30]S. Knight, S. Schöche, V. Darakchieva, P. Kühne, J.-F. Carlin, N. Grandjean, C. M. Herzinger, M. Schubert, and T. Hofmann, Opt. Lett. **40**, 2688 (2015).
[31]S. Knight, S. Schöche, P. Kühne, T. Hofmann, V. Darakchieva, and M. Schubert, Rev. Sci. Instr. **91**, 083903 (2020).
[32]N. Armakavicius, J.-T. Chen, T. Hofmann, S. Knight, K. Philipp, D. Nilsson, U. Forsberg, E. Janzén, and V. Darakchieva, Phys. Status Solidi C **13**, 369 (2016).

[33]P. Kühne, N. Armakavicius, V. Stanishev, C. M. Herzinger, M. Schubert, and V. Darakchieva, IEEE Trans. Terahertz Sci. Technol. **8**, 257 (2018).
[34]A. Kakanakova-Georgieva, S.-L. Sahonta, D. Nilsson, X. T. Trinh, N. T. Son, E. Janzén, and C. J. Humphreys, J. Mater. Chem. C **4**, 8291 (2016).
[35]M. Schubert, Phys. Rev. B **53**, 4265 (1996).
[36]I. Tan, G. L. Snider, L. D. Chang, and E. L. Hu, J. Appl. Phys. **68**, 4071 (1990).
[37]B. Jogai, J. Appl. Phys. **91**, 3721 (2002).
[38]P. Reddy, I. Btyan, Z. Bryan, J. Tweedie, S. Washiyama, R. Kirste, S. Mita, R. Collazo, and Z. Sitar, Appl. Phys. Lett. **107**, 091603 (2015).
[39]A. M. Armstrong and A. A. Allerman, Appl. Phys. Lett. **109**, 222101 (2016).
[40]J. W. Harrison and J. R. Hauser, Phys. Rev. B **13**, 5347 (1976).
[41]S. Schöche, T. Hofmann, D. Nilsson, A. Kakanakova-Georgieva, E. Janzén, P. Kühne, K. Lorenz, M. Schubert, and V. Darakchieva, J. Appl. Phys. **121**, 205701 (2017).
[42]U. Ekenberg, Phys. Rev. B **40**, 7714 (1989).
[43]B.-H. Wei and S.-W. Gu, Phys. Rev. B **43**, 9190 (1991).
[44]A. M. Kurakin, S. A. Vitusevich, S. V. Danylyuk, H. Hardtdegen, N. Klein, Z. Bougrioua, A. V. Naumov, and A. E. Belyaev, J. Appl. Phys. **105**, 073703 (2009).
[45]T. Ando, A. B. Fowler, and F. Stern, Rev. Mod. Phys. **54**, 437 (1982).
[46]S. Syed, J. B. Heroux, Y. J. Wang, M. J. Manfra, R. J. Molnar, and H. L. Stormer, Appl. Phys. Lett. **83**, 4553 (2003).
[47]S. Sarma and B. Mason, Ann. Phys. **163**, 78 (1985).
[48]F. M. Peeters, X. Wu, and J. T. Devreese, Phys. Rev. B **37**, 933 (1988).
[49]S. L. Rumyantsev, M. S. Shur, and M. E. Levinshtein, *GaN-Based Materials and Devices: Growth, Fabrication, Characterization and Performance*, edited by M. Shur and R. Davis (World Scientific, 2004), p. 1.
[50]J. T. Devreese, Phys. Scr. **T25**, 309 (1989).